Sol-gel Synthesis of One-Dimensional Photonic Bandgap Structures

by

Andrew William Sparks

Submitted to the Department of Materials Science and Engineering
in partial fulfillment of the requirements for the degree of

Bachelor of Science in Materials Science and Engineering

at the

MASSACHUSETTS INSTITUTE OF TECHNOLOGY

June 1999

Author .....
Department of Materials Science and Engineering
May 7, 1999

Certified by .....
Lionel C. Kimerling
Thomas Lord Professor of Materials Science and Engineering
Thesis Supervisor

Certified by .....
Kazumi Wada
Visiting Professor
Thesis Supervisor

Accepted by .....
Ronald M. Latanison
Professor of Materials Science and Engineering
Chairman, Undergraduate Committee

Sol-gel Synthesis of One-Dimensional Photonic Bandgap Structures

by

Andrew William Sparks

Submitted to the Department of Materials Science and Engineering
on May 7, 1999, in partial fulfillment of the
requirements for the degree of
Bachelor of Science in Materials Science and Engineering

Abstract

A series of one-dimensional photonic bandgap devices were fabricated using SiO_2 and TiO_2 films deposited from solution by the sol-gel method. A dielectric mirror, or broadband interference filter, was fabricated by alternating quarter-wave optical thickness layers of the two films on a silicon substrate for a total of six layer pairs. This device exhibited an omnidirectional photonic bandgap of 450 nm in TE-polarization and 110 nm in TM-polarization. A microcavity, or narrowband filter, was fabricated with a TiO_2 Fabry-Perot cavity sandwiched between two mirrors of three layer pairs each. The resonant cavity corresponded to a wavelength of roughly 1500 nm and shifted to shorter wavelengths with increasing incident angles. A maximum resonant quality factor of 11.7 was achieved.

Thesis Supervisor: Lionel C. Kimerling
Title: Thomas Lord Professor of Materials Science and Engineering

Thesis Supervisor: Kazumi Wada
Title: Visiting Professor

Acknowledgments

This work was supervised by Mr. Kevin Chen, Dr. Kazumi Wada, Dr. Jurgen Michel, and Professor Lionel Kimerling. The author thanks Mr. Thomas Chen, Mr. Andrew Luan, and Mr. Tim McClure for their assistance.

Contents

List of Figures

Chapter 1

Introduction

Photonic crystals have emerged in the past decade as a highly efficient means of guiding light on the submicron scale. These artificial crystals, also referred to as photonic bandgap (PBG) materials, exhibit a carefully engineered refractive index variation that excludes certain frequencies of light in the same manner that a semiconductor forbids certain electron energy states. This variation may occur in one, two, or three dimensions; successfully fabricated examples of each case are shown in Figure 1-1(a) and (b); Figure 1-1(c) is a proposed structure which has not yet been experimentally realized. With minimum feature sizes on the order of hundreds of nanometers for applications in the infrared regime, PBG materials promise to be of great importance to the telecommunications and computer industries.

1.1 Background

A comprehensive discussion of the theory of photonic crystals can be found in Reference [1]. Photonic crystals can best be understood by comparison with semiconductors. In a semiconductor, a bandgap arises from a periodic lattice potential that causes electrons to scatter off atoms. In a photonic crystal, a periodic refractive index variation changes the energy of photons propagating through the material. Photons scatter off the interfaces between regions of contrasting indices, resulting in a photonic bandgap.

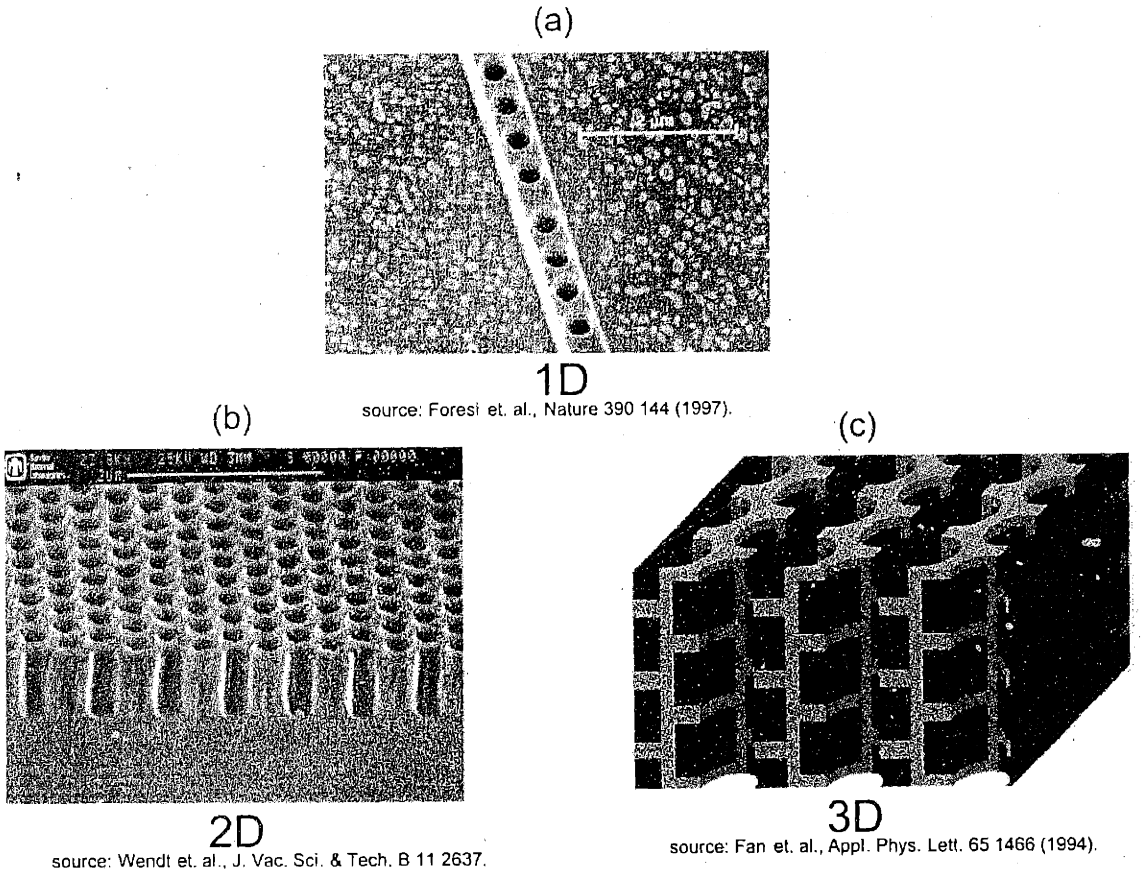

Figure 1-1: *(a) 1D, (b) 2D, and (c) 3D photonic crystals.*

Ideally, a photonic bandgap would exist for all directions of incidence upon a crystal. Such a material must exhibit a refractive index variation, or dielectric contrast, in all directions, i.e. it must be a three-dimensional photonic crystal. Although several structures have been successfully demonstrated, they all require sophisticated fabrication techniques such as electron beam lithography [2]; their feasibility is questionable.

Recently, it has been predicted [3] and experimentally realized [4] that a one-dimensional photonic crystal (Figure 1-2), which is essentially a multilayered composite, of an appropriate dielectric contrast can possess an omnidirectional photonic bandgap: any angle of incidence will serve to exclude some constant range of frequencies (Figure 1-3). Thus it serves as a broadband filter, or dielectric mirror, for that frequency range. A high dielectric contrast is necessary to strongly deflect the "forbidden" frequencies of light and will increase the size of the gap. By introduc-

ing a "defect" layer, or Fabry-Perot microcavity, of unique thickness in an otherwise periodic structure, a certain mode of light within the forbidden frequency range can resonate within the material, creating a narrowband filter (Figure 1-4). Such a structure is useful in selecting a signal in wavelength division multiplexing (WDM), when multiple signals can propagate simultaneously at different wavelengths along a waveguide.

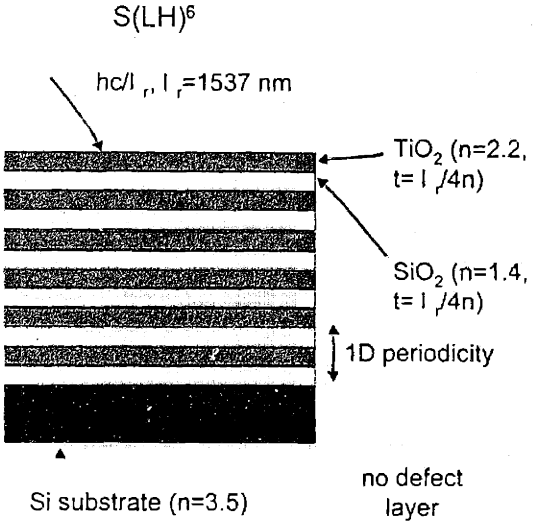

Figure 1-2: *The $S(LH)^6$ dielectric mirror.*

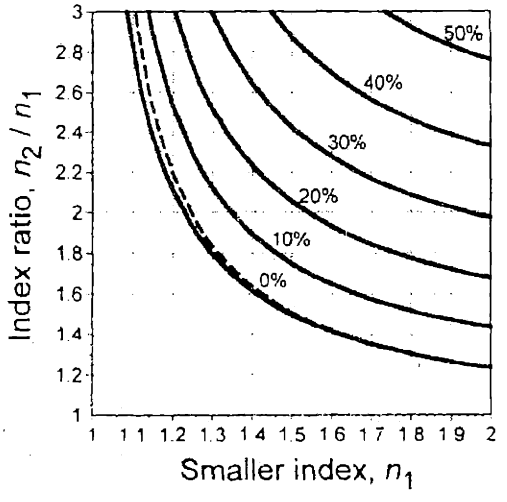

Figure 1-3: *The omnidirectionality condition (Winn et. al., Opt. Lett. 23 1573 (1998)).. The contours represent the value $\frac{2(\lambda_1-\lambda_2)}{\lambda_1+\lambda_2}$, where λ_1 and λ_2 are the lower and upper bounds of the photonic bandgap, respectively.*

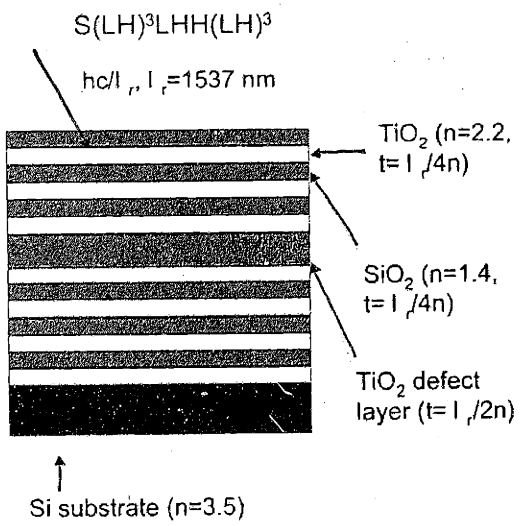

Figure 1-4: *The $S(LH)^3L(2H)(LH)^3$ microcavity.*

Reflectance spectra of these multilayer stack structures for light at normal incidence can be predicted using the transfer matrix method [5]. This technique calculates the vector sum of the electric and magnetic fields incident, reflected, and transmitted at each interface. It works for any multilayer configuration and accounts for the refractive index and thickness of each layer as well as any defect layers. The code was written by Thomas Chen.

1.2 Synthesis

One-dimensional photonic crystals are fabricated primarily by physical or chemical vapor deposition techniques, but these are expensive, time-intensive, and area-limited techniques. The sol-gel method is more attractive for this function because it requires only a standard chemical bench, spin-coater, and furnace, and because it allows deposition of uniform oxide films at temperatures less than 1000°C.

The sol-gel process [6,7] is illustrated in Figure 1-5. A solution is prepared containing a metal alkoxide that incorporates the elements of the oxide. Also present in solution is water, which slowly hydrolyzes the metallorganic compound in a step polymerization process, and an alcohol, which encourages the reaction of the immiscible alkoxide and water. A chelating agent, typically an amine with large sidechains,

1. Hydrolysis

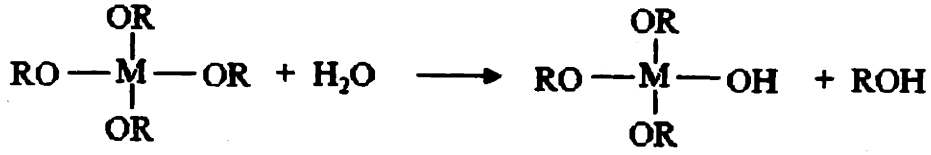

2. Condensation/Polymerization

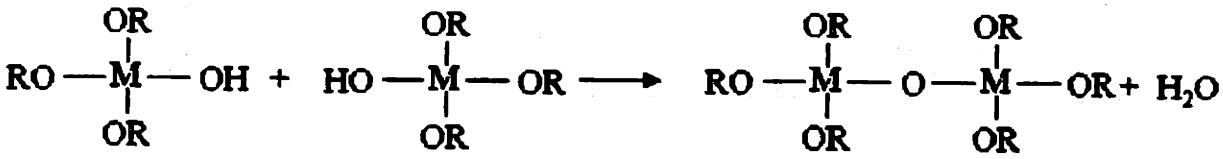

3. Heat Treatment

Figure 1-5: *The sol-gel process (M=metal).*

may also be added to control the hydrolysis reaction kinetics. After the solution is spun onto the wafer, it further hydrolyzes by reacting with water vapor and polymerizes until it forms a three-dimensional solvent-swollen continuous oxide network, or gel. The gel is dried and fired to burn off residual organic compounds and densify the network into a uniform, amorphous oxide. Subsequent heat treatment can cause crystallization, but for optical applications amorphous coatings are preferred to minimize scattering.

SiO_2 and TiO_2 were investigated for device applications because of their roles as common sol-gel films. They were selected because they provide the maximum dielectric contrast for single cation oxides (refractive indices of about 1.4 and 2.4, respectively, have been experimentally observed for amorphous films). This contrast suggests an omnidirectional photonic bandgap of roughly 150 nm (Figure 1-3).

Chapter 2

Experimental Procedure

Several one-dimensional photonic bandgap structures were fabricated for operation at wavelengths in the vicinity of 1537 nm, the standard for integrated photonics and silicon-based optoelectronics. In the notation to describe these structures, "L" indicates the quarter wave optical thickness (QWOT) $\frac{\lambda_r}{4n}$, where λ_r is the wavelength in the middle of the projected bandgap, 1537 nm, and n is the refractive index of the lower index component (SiO_2). "H" indicates the QWOT of the higher index component (TiO_2) and "S" indicates the silicon substrate. Exponents represent repeat units.

2.1 Device Design

For the defect-free dielectric mirror, simulations predicted that increasing the number of layer pairs (LH) sharpens the band edges. However, since a heat treatment was performed after each deposited layer, cracks from thermal stresses appeared on the devices after several layers which lowered the optical quality of the films. These scattering sites could particularly affect the performance of the filter at non-normal angles of incidence. To reduce the number of cracks and the overall processing time of the device, an $S(LH)^6$ structure was selected for fabrication. A higher index layer appeared on top of the structure to increase the reflectivity of the surface of the device. The theoretical spectrum is shown in Figure 2-1.

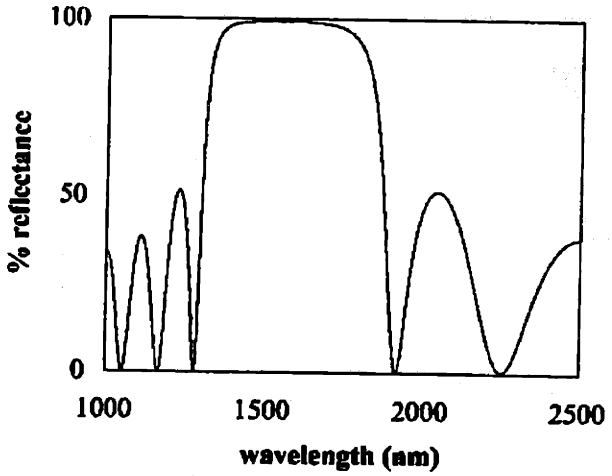

Figure 2-1: *Theoretical reflectance spectrum of the* $S(LH)^6$ *dielectric mirror.*

Defect layers of $(2H)$ were used in the microcavity filters to obtain a resonant peak in the middle of the bandgap. The $(2H)$ defect layer creates standing waves of wavelength λ_r, trapping the light within the film. The thickness of the defect layer can be altered to shift the resonant peak to higher or lower wavelengths. A TiO_2 defect layer was selected over SiO_2 because of the slightly higher optical quality of the TiO_2 films deposited and thus its ability to more efficiently confine light. $S(LH)^3L(2H)(LH)^3$ and $S(LH)^4L(2H)(LH)^4$ structures were selected to minimize the reflectance at the resonant wavelength and the full-width at half-maximum (FWHM) of the peak (Figure 2-2), and also to restrict the total number of layers to a reasonable number.

2.2 Solution Preparation

SiO_2 solutions were synthesized according to a recipe reported by Fabes et. al. [8]. All chemical preparation occurred under an argon atmosphere to prevent premature hydrolysis. One molar equivalent of tetraethoxysilane (TEOS) was mixed with four

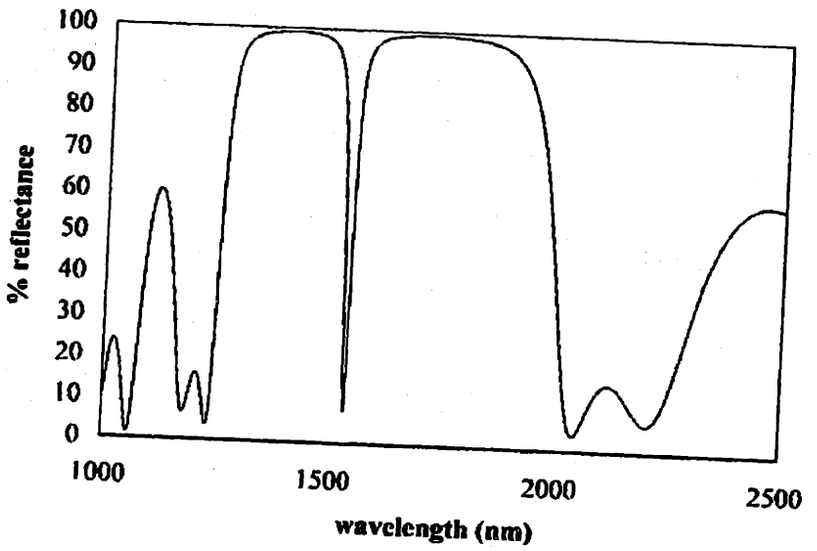

Figure 2-2: *Theoretical reflectance spectrum of the* $S(LH)^3L(2H)(LH)^3$ *microcavity.*

equivalents of ethanol, and the solution was hydrolyzed by adding two equivalents of acidified water (0.36 M HCl) to yield a pH of 2, the isoelectric point (IEP) of silica solutions. The IEP is the point at which the silica particles that form exhibit no electrical mobility, and thus the reaction kinetics are minimized and the solution lifetime is maximized [6]. This is also the approximate point of zero charge (PZC), where protons are not added or removed from the alkoxide and the kinetics are further minimized [6].

TiO_2 solutions were prepared according to Selvaraj et. al. [9]. 1 equivalent of titanium isopropoxide ($Ti(OPr^i)_4$) was dissolved in 5 equivalents anhydrous isopropanol under an Ar atmosphere. Because the titania precursor is highly reactive, one equivalent of diisopropanolamine was added to this solution as a chelating agent, followed by 4 more equivalents of isopropanol mixed with 2 equivalents of water.

2.3 Single Film Characterization

Single films of SiO_2 and TiO_2 were spun onto silicon substrates at 4500 rpm for 30 seconds to get the desired QWOT. Two heat treatments were tested for each type of film: 1) two minute dry at 100°C, fifteen minute fire at 500°C, and ten minute cooldown at 100°C; and 2) two minute dry at 200°C, fifteen minute fire at 700°C, and ten minute cooldown at 200°C. The firing temperatures were selected from a literature survey: a lower firing temperature would result in overporous, low refractive index films, but a higher firing temperature could result in thermal stresses between films and possible crystallization of TiO_2 films [8,9].

Optical microscopy results are shown in Figure 2-3. The circular imperfections on the film surfaces are scattering sites; they are thought to be pores. Though prevalent at 500°C, at 700°C the network densifies enough to virtually eliminate them. Furthermore, no cracks are present on the 700°C films. All devices were therefore fabricated using the second heat treatment procedure for each layer pair.

2.4 Layer Calibrations

Film thickness calibration was necessary to ensure very precise and reproducible layer thicknesses could be obtained. Because silicon has a native oxide layer of around 50 Å, calibrations for both films were performed on silicon substrates; the viscosities of the solutions were roughly equal and the surface tensions of the dried and fired films and the native oxide were similar enough that it was not necessary to calibrate SiO_2 on TiO_2 and vice versa [10].

Optical thicknesses of the films were determined by ellipsometry (Gaertner) using 632.8 nm laser light. All spin-coatings were done for 30 seconds. Although QWOTs corresponding to a wavelength of 1537 nm were desired, layer detuning [11] simplified the process of finding spin speeds that would give the exact optical thicknesses. The detuning concept suggests that, for PBG structures at normal incidence, it is not important that each layer thickness be equal to the QWOT, but that each layer pair

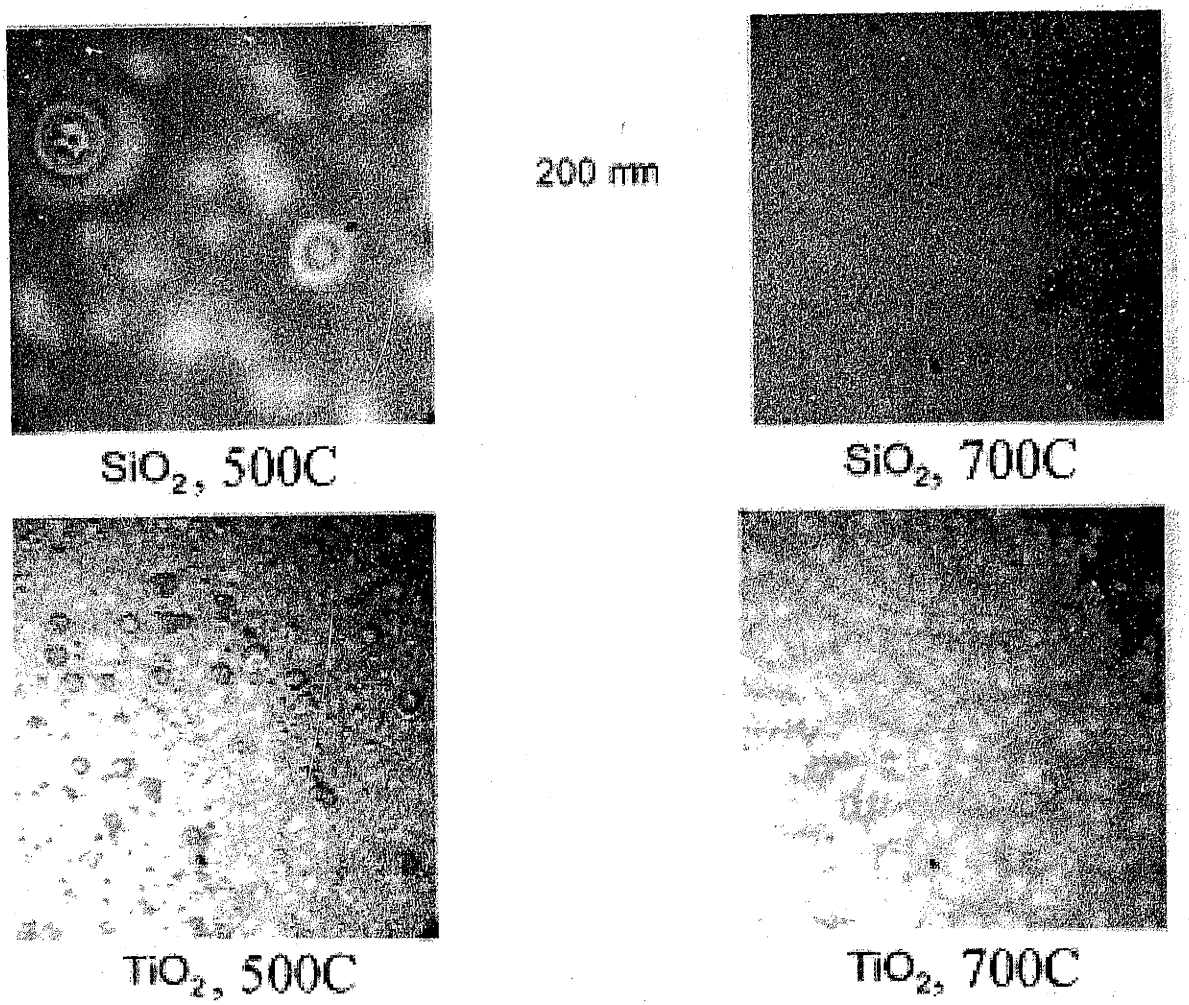

Figure 2-3: *Optical micrographs of single films of SiO_2 and TiO_2 at 500° C and 700° C heat treatment temperatures.*

be equal to the average half wave optical thickness, $\frac{\lambda_r}{n_{SiO_2}+n_{TiO_2}}$. However, since this was not confirmed for off-normal incidence, film thicknesses were kept as close to the QWOTs as possible.

Each solution synthesized was calibrated independently of previously synthesized solutions. Since the degree of polymerization of the solutions increases with time, film calibrations were performed before each device was fabricated. However, for both solutions, 4500 rpm was used throughout the project to obtain films of near the desired thickness.

2.5 Reflectance Spectra Measurements

Reflectance spectra for each device were obtained using Fourier Transform Infrared Spectroscopy (FTIR, Nicolet) over a wavelength range of 1000 nm to 2500 nm. A white light source was used with a 5 mm aperture, a CaF_2 beam splitter and a HgCdTe infrared detector. Gold was used as a reflectance standard. For off-normal incidence measurements, reflectance was tested up to 80°, the highest angle achievable.

Chapter 3

Results and Discussion

3.1 The Dielectric Mirror

The reflectance spectrum for the $S(LH)^6$ dielectric mirror at normal incidence is in Figure 3-1. All spectra have been normalized to 100% reflectance – although they are more reflective than the gold standard, the maximum obtained reflectance value fluctuates with no apparent angular dependence. A photonic bandgap of 450 nm is observed, just short of the 470 nm gap predicted. At normal incidence, the spectral profile is very similar to the theoretical prediction but is shifted to higher wavelengths by about 10%. Although calibrated for a resonant wavelength of 1537 nm, the average QWOT is actually closer to 1600 nm, resulting in the spectral shift. It is difficult to calibrate accurately because each layer needs to be heat treated before subsequent depositions, so layers toward the bottom of the stack will be slightly more densified and will have smaller thicknesses. Although denser films have higher refractive indices, which partially compensates for the shrinkage [12], the spectral profile still appears to be affected by optical thickness variations.

For off-normal incidence, spectral analysis was broken into transverse electric (TE) polarized light (Figure 3-2) and transverse magnetic (TM) polarized light (Figure 3-3). TE modes exhibit an omnidirectional photonic bandgap of 410 nm, while TM modes exhibit a 110 nm gap. For light of any polarization within this 110 nm gap, the device acts as a near perfect mirror: without losses and thus more reflective than

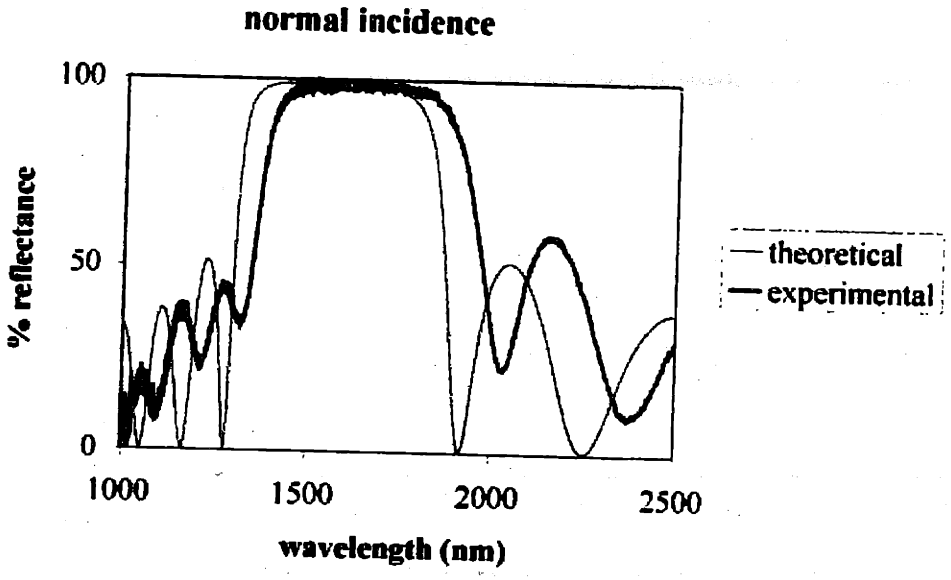

Figure 3-1: *Reflectance of the $S(LH)^6$ dielectric mirror at normal incidence.*

gold. This is in close agreement with the 150 nm gap suggested by Figure 1-3 for the refractive indices of this system.

3.2 The Microcavity

The normal incidence spectrum for the $S(LH)^3L(2H)(LH)^3$ microcavity is displayed in Figure 3-4. The devices are characterized by a resonant quality factor,

$$Q = \frac{\Delta\lambda_{gap}}{\Delta\lambda_{peak}} = \frac{bandgap\_width}{FWHM}, \tag{3.1}$$

where FWHM is the full-width at half-maximum of the resonant peak. Two different samples of this device structure were fabricated and measured; their spectral profiles are close to each other and somewhat similar to the theoretical reflectance spectrum, but the peaks are shifted to slightly shorter wavelengths. This is because of an inaccurate calibration of the defect layer. It can be seen that changing the defect layer thickness changes the placement of the resonant peak in the bandgap, as predicted. The quality factors of these samples are 11.7 and 7.3, respectively, less than the

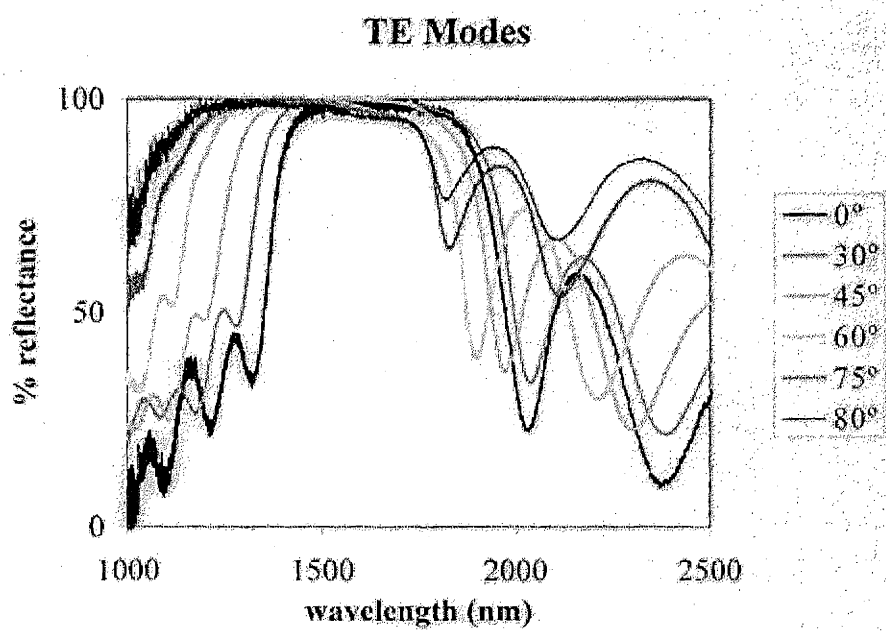

Figure 3-2: *TE reflectance of the $S(LH)^6$ dielectric mirror.*

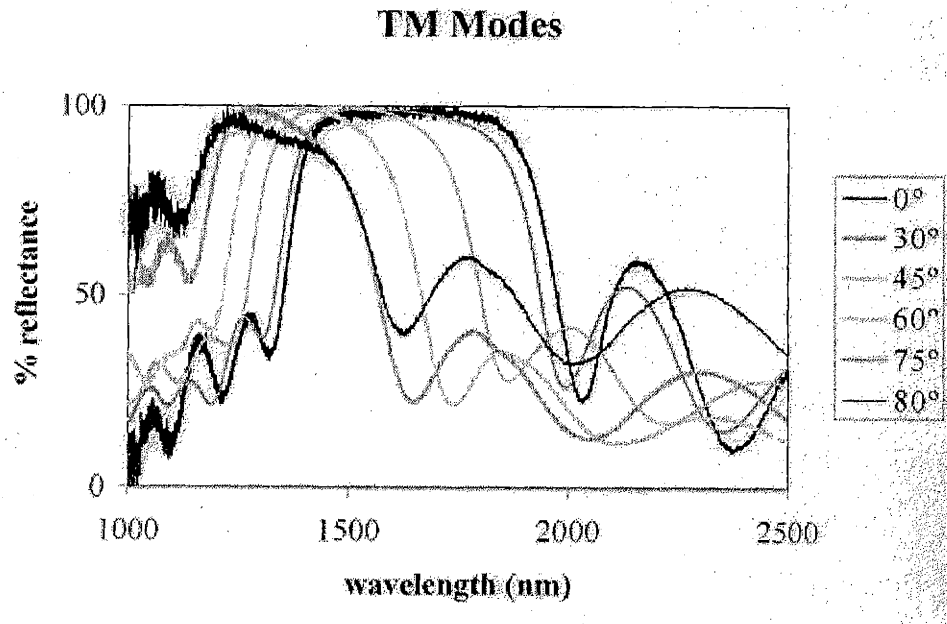

Figure 3-3: *TM reflectance of the $S(LH)^6$ dielectric mirror.*

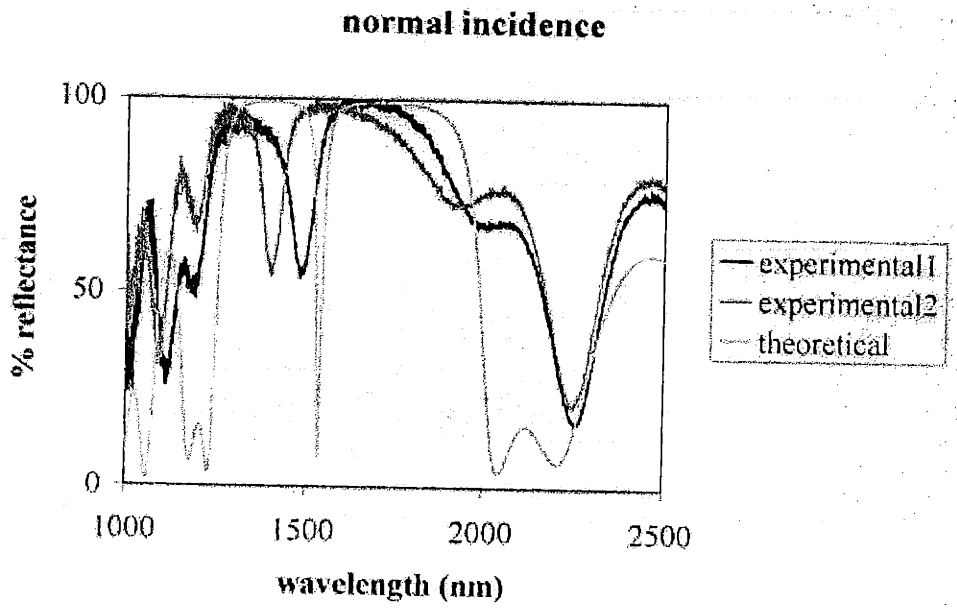

Figure 3-4: *Reflectance of the* $S(LH)^3L(2H)(LH)^3$ *microcavity at normal incidence.*

predicted 37.5 by factors of 4 to 5.

For TE-polarized light (Figure 3-5), as the angle of incidence increases the resonant peak shifts to shorter wavelengths, from about 1500 nm at normal incidence to 1300 nm at 80° incidence. Although there is some decrease in Q as the angle increases, the peak shift is very useful for narrowband filtering applications: simply rotating the device can result in different wavelengths of light reflecting or transmitting. TM-polarized light (Figure 3-6) shows a similar peak-shifting effect, but the peaks disappear at high angles of incidence.

The $S(LH)^4L(2H)(LH)^4$ devices show similar patterns, though not as prominently. More importantly, the Q of the device at normal incidence (Figure 3-7) stays about the same as the $S(LH)^3L(2H)(LH)^3$ devices, although it was predicted to increase to about 70. Furthermore, at non-normal incidence the peaks are less pronounced for both TE (Figure 3-8) and TM (Figure 3-9) polarizations and become obscured at large angles. These results suggest that the optimal extent of the fabrication process has been realized for the $S(LH)^3L(2H)(LH)^3$ devices. In other words, increasing the number of layer pairs does not improve device performance, probably

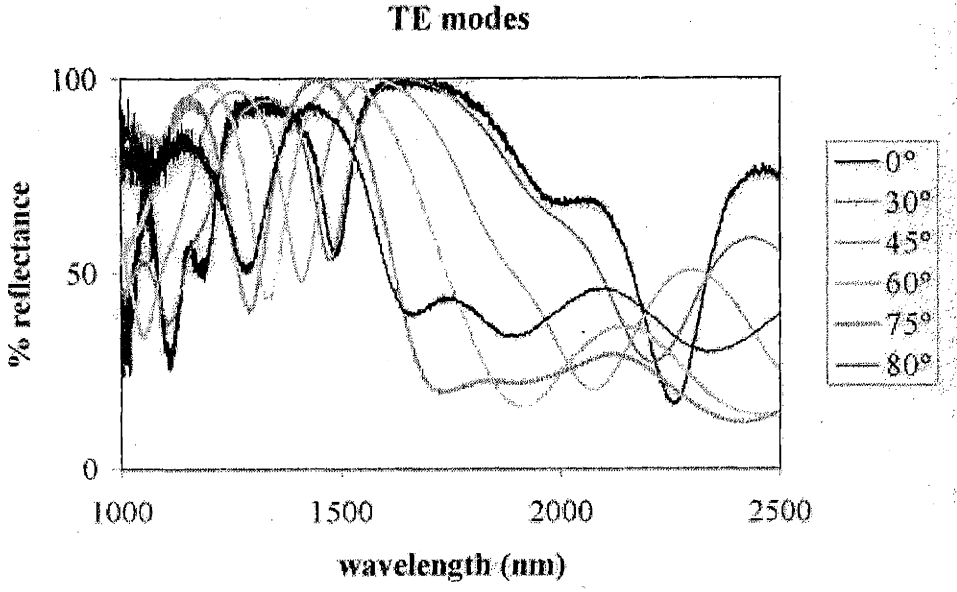

Figure 3-5: *TE reflectance of the* $S(LH)^3L(2H)(LH)^3$ *microcavity.*

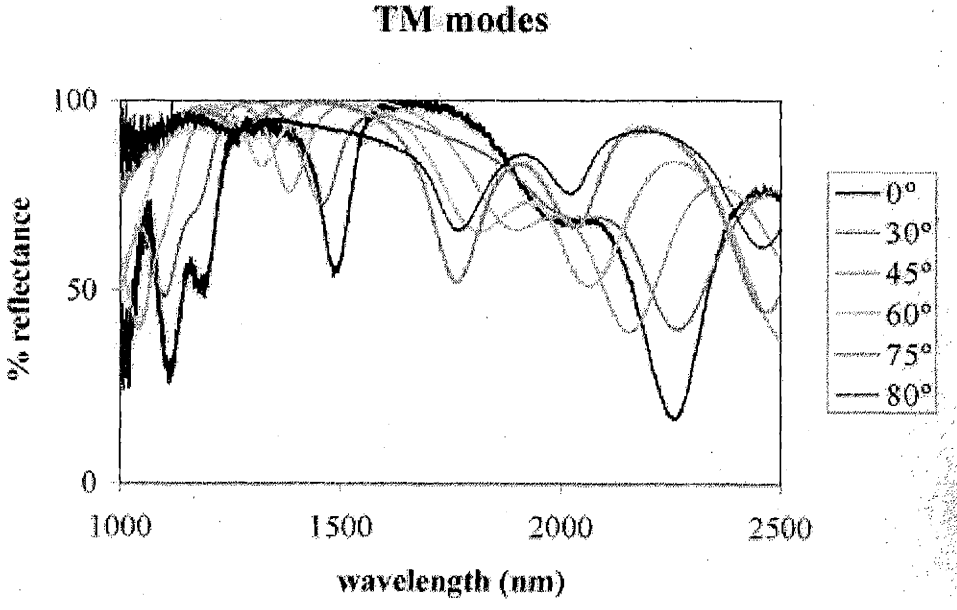

Figure 3-6: *TM reflectance of the* $S(LH)^3L(2H)(LH)^3$ *microcavity.*

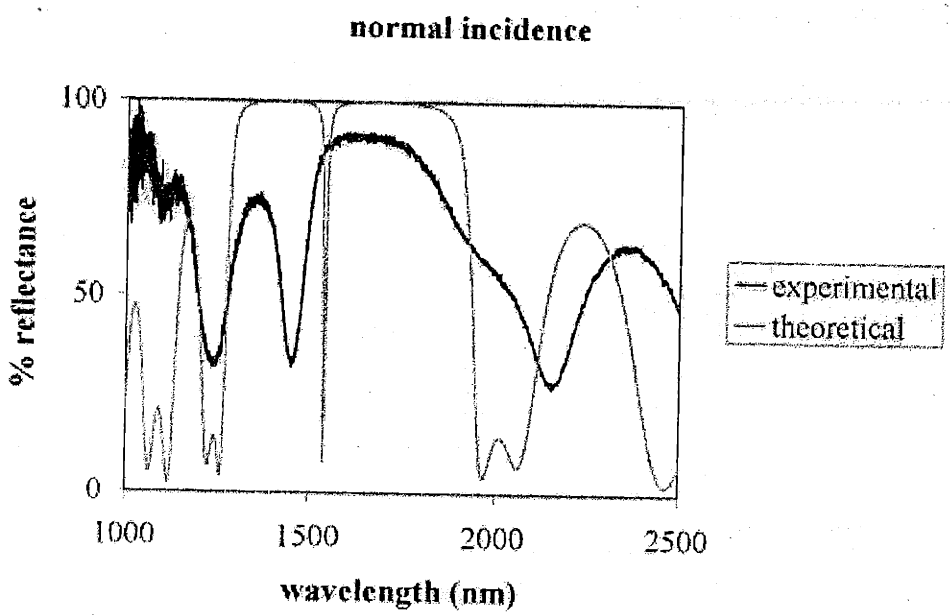

Figure 3-7: *Reflectance of the* $S(LH)^4L(2H)(LH)^4$ *microcavity at normal incidence.*

due to thermal stresses between films near the bottom of the structures that generate scattering sites.

The overall imperfect behavior of the microcavity devices can be explained by the presence of the defect layer. For the dielectric mirror, the structure was completely periodic and thus slight deviations in layer thicknesses and film quality went unnoticed in the reflectance spectra. However, with the addition of a defect layer, the lack of complete periodicity means that there is no large scale correction for these kinds of deviations.

Despite the non-ideal device behavior, the realization of such structures by the sol-gel method is important. Q values may be too low for WDM but many filter applications may not have such strict requirements, and sol-gel filters would be economically advantageous.

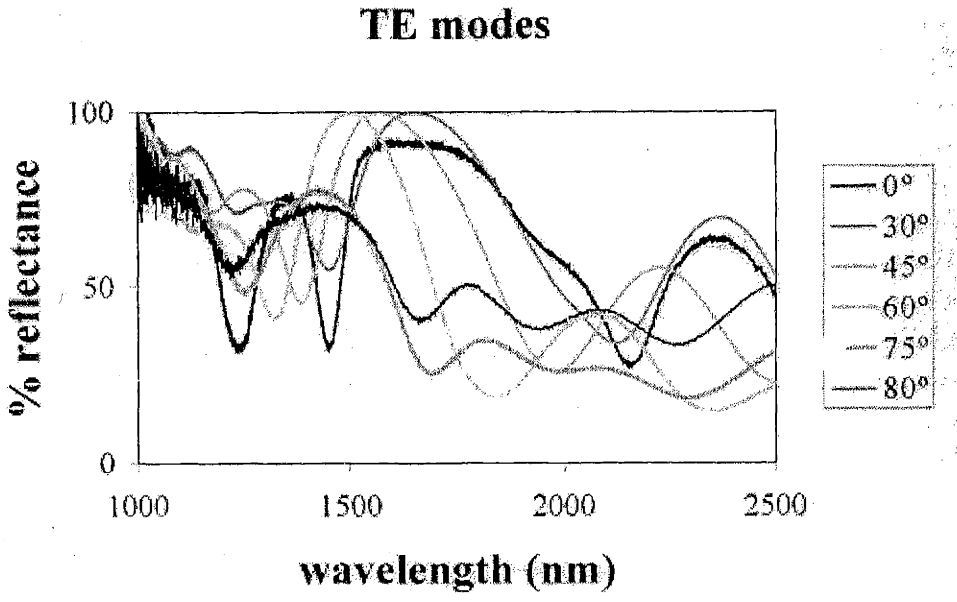

Figure 3-8: *TE reflectance of the* $S(LH)^4L(2H)(LH)^4$ *microcavity.*

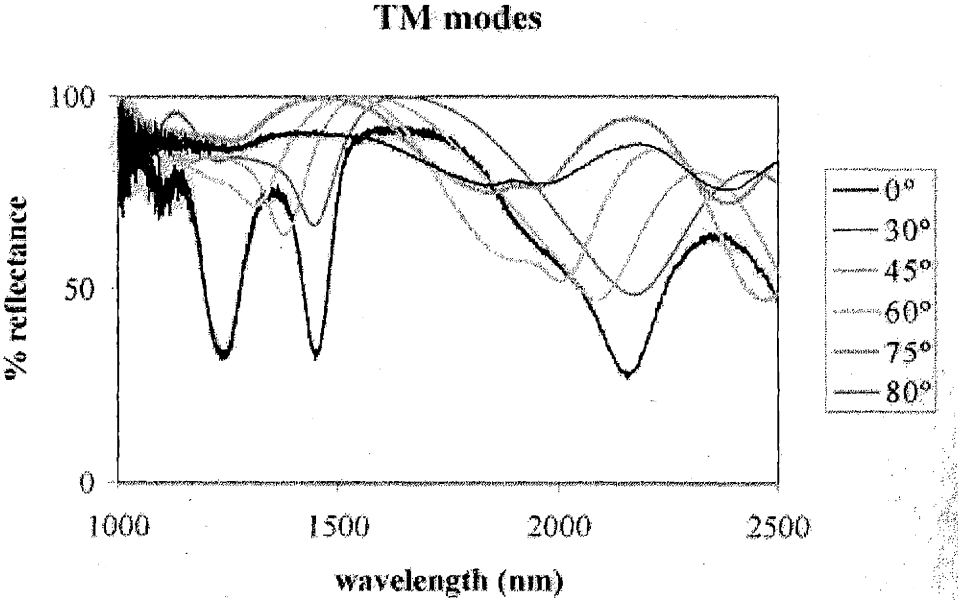

Figure 3-9: *TM reflectance of the* $S(LH)^4L(2H)(LH)^4$ *microcavity.*

Chapter 4

Conclusions

4.1 Achievements

There are several notable accomplishments of this work. The first is the establishment and optimization of a process for building multilayer optical devices via the sol-gel method. This includes the synthesis of both SiO_2 and TiO_2 solutions and the refinement of a heat treatment process for thin oxide films. The process developed has laid the foundation for future work in one-dimensional PBG structures and related devices.

Secondly, this research was the first known confirmation of an omnidirectional photonic bandgap in a sol-gel dielectric stack. It promises to be an economically advantageous alternative to previously demonstrated metal-polymer [4] and semiconductor-oxide [13] devices.

Thirdly, this work is the first known demonstration of a sol-gel microcavity. Although the predicted spectral characteristics could not entirely be achieved, improving processing conditions, e.g. the argon atmosphere under which the solutions were prepared and the furnace used for heat treatments, is expected to yield better films and higher performance devices.

Finally, this project is the first association of photonic crystal research with sol-gel technology. Current research involves the use of sol-gel films as matrices for three-dimensional PBG devices and will certainly be extended to include other approaches

to photonic crystal fabrication.

4.2 Future Work

Efforts are underway to build optical amplifiers and electro-optic modulators from these basic devices. The optical amplifier is made possible by doping the defect layer with Er^{3+}, presumably by doping the SiO_2 and/or TiO_2 solutions with an erbium organic precursor to yield Er_2O_3 in the oxide films [14]. Er^{3+} ions could be optically pumped such that 1537 nm light localized in the defect layer is amplified by a stimulated emission mechanism.

An electro-optic modulator can be fabricated by using an electro-optic crystalline film as a defect layer. A $BiSr_2Ta_2O_9$ (BST) sol-gel solution has been acquired from the Tokyo Institute of Technology for this purpose, although the defect layer will require a more involved heat treatment procedure in order to crystallize the BST. Applying an electric field across this layer on the order of 1 V will result in a change in the optical thickness, thus shifting the peak and modulating the reflectance behavior of the device.

This work has provided a template for the construction of these more advanced photonic bandgap devices with the economic advantages of the sol-gel method.

Bibliography

[1] J. D. Joannopoulos, R. Meade, and J. N. Winn, *Photonic Crystals: Molding the Flow of Light* (Princeton Univ. Press, Princeton, NJ, 1995).

[2] J. D. Joannopoulos, P. R. Villenueve, and S. Fan, *Nature* **386** 143 (1997).

[3] J. N. Winn, Y. Fink, S. Fan, and J. D. Joannopoulos, *Opt. Lett.* **23** 1573 (1998).

[4] Y. Fink, J. N. Winn, S. Fan, C. Chen, J. Michel, J. D. Joannopoulos, and E. L. Thomas, *Science* **282** 1679 (1998).

[5] G. R. Fowles, *Introduction to Modern Optics* (Dover Press, Mineola, NY, ed. 2, 1975), p. 98.

[6] C. J. Brinker and G. W. Scherer, *Sol-Gel Science: The Physics and Chemistry of Sol-Gel Processing* (Academic Press, New York, 1990).

[7] A. C. Pierre, *Introduction to Sol-Gel Processing* (Kluwer Academic Publishers, Boston, 1998).

[8] B. D. Fabes, D. P. Birnie III, B. J. J. Zelinski, *Thin Solid Films* **254** 175 (1995).

[9] U. Selvaraj *et. al., J. Am. Ceram. Soc.* **75** 5 1167 (1992).

[10] Q. Wu *et. al.*, in *Ceramic Transactions* (American Ceramic Society, Westerville, OH, 1995), p. 235.

[11] Z. Knittl, *Optics of Thin Films: An Optical Multilayer Theory* (Wiley, London, 1976).

[12] P. K. Biswas, D. Kundu, D. Ganguli, *J. Mat. Sci. Lett.* **6** 1481 (1987).

[13] J. S. Foresi, P. R. Villenueve, J. Ferrera, E. R. Thoen, G. Steinmeyer, S. Fan, J. D. Joannopoulos, L. C. Kimerling, H. I. Smith, and E. P. Ippen, *Nature* **390** 143 (1997).

[14] A. Bahtat, M. Bouazaoui, M. Bahtat, J. Mugnier, *Optics Comm.* **111** 55 (1994).